

Lung Cancer Detection Using Deep Convolutional Neural Networks

^{1*}Laxmikant Tiwari, ²Rohit Raja, ³Vineet Awasthi, ⁴Rohit Miri, ⁵Akanksha Gupta

¹Research Scholar, Department of CSIT, Dr. C. V. RAMAN University, Bilaspur, India,
laxmikant.tiwari@gmail.com

²Associate Professor, Department of IT, GGV Central University, Bilaspur, India,
drrohitraja1982@gmail.com

³Professor, Department of Information Technology, Dr. C. V. RAMAN University Bilaspur, India

⁴Professor, Department of Information Technology, Dr. C. V. RAMAN University Bilaspur, India,
rohitmiri@gmail.com

⁵Assistant Professor, Department of Information Technology, GGV Central University, Bilaspur Central University India.

Abstract:

Lung Cancer growth is one of the significant reasons for disease-related Deaths because of its forceful nature and postponed identifications at cutting edge phases. Primary identification of lung disease is substantial for the endurance of a person and remains a critical testing issue. Most chest radiographs (X-beam) and recorded tomography (CT) scans are used at first to assess the hazardous knobs; in either event, the possible existence of polite keys prompts inappropriate decisions. At the initial phases, the nice and fragile knobs are next to each other. Here, a new, profound learning-based paradigm with different approaches is suggested to examine the dangerous knobs exactly. Owing to ongoing achievements in in-depth convolutionary neural systems (CNN) in picture analysis, we used two extreme three-dimensional (3D) altered blended relation arrangement (CMixNet) constructs independently for lung knob exploration and characterization. Knob recognition was performed via faster R-CNN on effectively taking highlights from CMixNet and U-Net like encoder-decoder engineering. Characterization of the knobs was accomplished by an orientation boosting machine (GBM) on the outlines of the intended 3D CMixNet layout. To reject false positive outcomes and misdiagnosis due to various mistake types, an acceptable urge was acted on clinical side effects and clinical pathogenesis. Through the network of things (IoT) approach and electro-clinical engineering, remote body popular frameworks (WBANs) provide reliable patient management, helping to decide endless diseases — particularly metastatic sicknesses. The deep neural network for identification and classification of knobs, related to clinical components, begins to reduce disorder, and false optimism (FP) contributes to discovering the initial step of lung disease. The suggested system was tested as affectability (94%) and explicitness (91%) on LIDC-IDRI datasets, and better findings were obtained in comparison to current techniques. In this article, we analyze the consistency of a deep learning technique to diagnose lung disease on clinical image analysis problems. Convolutionary neural systems (CNNs) have become popular within example recognition and PC vision testing territories as a function of their encouraging impact on substantial level representations.

Keywords: Computerized tomography; Deep Neural Network; Image Recognition; lung Cancer; clinical imaging

1. Introduction:

As specified by the World Health Organization (WHO) the lung malignancy is named a non-communicable illness, and it is the fifth reason for death (related to windpipe and bronchus disease) among every single imaginable reason assessed on the planet ("GHO |," n.d.). Lung Cancer growth is the most widely recognized kind of disease influencing the lives of numerous individuals worldwide for a very long while, which reasons for death are evaluated for almost 1.59 million individuals every year. As per Siegel (Siegel et al., 2014) is normal for 2017 that lung Cancer growth, among all tumors, presents the most noteworthy occurrence for new cases (222,500 cases) thinking about people as one gathering, and the most elevated mortality (155,870 Deaths) for the two sexual orientations in

the United States. Among people, it will be the second reason for death, losing only for prostate Cancer growth for men and bosom disease for ladies (Siegel et al., 2014). Considering every single imaginable reason for death, it is watched, that lung disease has a higher occurrence on North America and Europe (Ferlay et al., 2015) (*GHO | By Category*, n.d.-b). It is accounted for that 58% of the lung cancer growths happened in less created nations (Ferlay et al., 2015) (Jemal Lindsey Torre Isabelle Soerjomataram Freddie Bray & Adams, n.d.). As per (Jemal Lindsey Torre Isabelle Soerjomataram Freddie Bray & Adams, n.d.), lung Cancer growth cause one of every five disease Deaths around the world (1.6 million Deaths, 19.4% of all Cancer growth Deaths). Thinking about these insights and the chance of augmentation of the reality eminence or remedy for early discovery (*Early Detection of Lung Cancer | F1000Research*, n.d.), it is imperative to contribute to frameworks for initial lung Cancer growth location. The Main Lung Screening Trial revealed a 20 % decrease in mortality, despite low-processed tomography screening (Midthun, 2016). Typically, as lung cancer development is predictive, it is ahead of time (Midthun, 2016) (Veronesi et al., 2014), thus adding to danger clumps testing could minimize deaths[19]. We can create optimization methods and patient tolerance by partnering with a licensed aided demonstrative (CAD) system to the traditional symptomatic process (Veronesi et al., 2014)(Midthun, 2016). Neural structures have been used to resolve CAD constructs (Kuan et al., n.d.)(Jadhav et al., 2015)(Taher & Sammouda, 2011), providing encouraging performance. As such, clinical picture analysis suggests substantial early detection of such disease from clinical pictures. This area of research can generally be organized in two forms of undertakings: division; the option of a questionable division that recognized as cancer growth and characterization; who use to infer and additionally assess a kind of disease; and, in certain cases, whether or not a person is under the cancer growth threat (known as conventional gathering).

Clinical image analysts have become particularly excited about developing lung cancer development inference techniques based on deep learning approaches. Intense learning strategy is an enhanced version of false neural networks, which consists of a few layers of high-demand highlights from its data, and then draws the anticipated opportunity on the machine brain. Within deep learning approaches, convolutionary neural networks (CNNs) have been commonly used in PC vision assignments. CNN's' implications have shown its influence in object-recognition weakness in various photographs. The implemented deep learning techniques are often established late in the clinical image investigative process. The greater part of interesting scholarly research works applied to achieve the display of clinical pictures is implemented either by modifying the architecture of the existing deep learning systems or by proposing new models.

Persuaded by the accomplishment of profound learning, our work focuses on getting familiar with an elevated level and discriminative element utilizing by CNN to analyze lung cancer growth. To address this issue, we propose another profound convolutional neural system (dCNN) engineering. Our machine protected three convolution layers, max-pooling layers, a full-related layer, and a double delicate max layer. This system starts with two consecutive convolution layers to create high-request highlights at the primer layers. At that point, the produced highlight maps go through different layers to the head of the system. To approve the exhibition of our dCNN, we test it on the KDSB17 informational collection. The trial results show that our dCNN perform amazingly, truth be told, it fundamentally beats numerous all the Kaggle contender's strategy in lung malignant growth determination picture examination task.

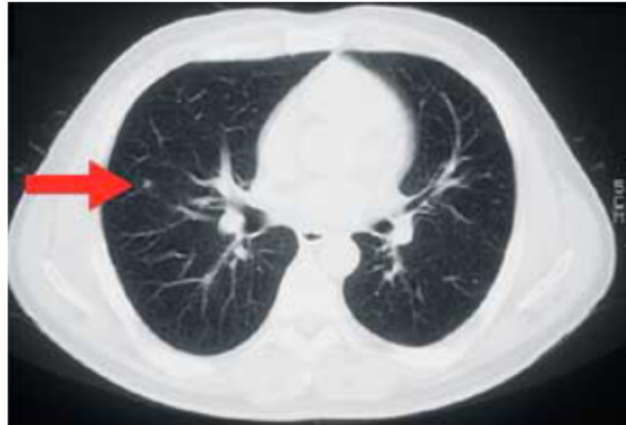


Fig 1: Show 2D CT scan contains a small (5mm) early-stage lung cancer nodule

2. Related Work:

Although the primary PC supported location (CAD) framework for lung knob identification was structured in the last part of the 1980s, these endeavors were not engaging because of insufficient computational assets for cutting edge picture examination methods around then. After the development of the graphical preparing unit (GPU) and convolutional neural systems (CNN), the exhibition of PC based picture examination and choice emotionally supportive network got a high lift. Analysts have proposed a great deal of profound learning-based clinical picture examination models, and a couple of the most significant lung knob discovery and characterization strategies are referenced here.

Setio et al. proposed a 3D, completely convolutional neural system for FP decrease in lung knob arrangement (Setio et al., 2017). A 3D mechanism utilized to break down the 3D idea of the CT outputs to diminish the wrong conclusion and weighted examination was used to improve results.

Ding and Liao et al. utilized 3D Faster R-CNN for knob discovery to diminish bogus positive (FP) aftereffects of lung Cancer growth determination (Zhu et al., 2018). Quicker R-CNN generally shows excellent outcomes for object identification. It was utilized with exceptionally profound present-day CNN engineering, the double way arranges (DPN), to become familiar with the highlights of the knobs for characterization (Ren et al., 2017).

Jiang Hongyang et al. intended to collect pneumonic knob identification using multi-patches to conspire with the Frangi platform to assist the presentation (Jiang et al., 2018). Pictures from both classes were combined and a four-channel 3D CNN was introduced to familiarise with the radiologist's highlights. The results of their CAD process indicate 80.06 percent affectability with 4.7 FP per sweep and 94 percent affectability with a 15.1 FP rate.

Zhu Wentao et al. proposed computerized lung knob identification and order models. They used 3D DPN with 3D quicker R-CNN and slope boosting machine (GBM) to identify lung knobs. (Zhu et al., 2018) The model shows an identification precision of 87.5% with a mistake pace of 12.5%.

Gu Yu et al. Proposed 3-D profound CNN with multiscale forecast techniques for the recognition of lung knobs from fragmented pics (Y. Et al., 2018). The 3D CNN performs much preferable with more extravagant highlights over 2D CNN. Notwithstanding 3D CNN, a multiscale lung knob forecast procedure was applied for the little knobs with robust shape grouping strategies.

Zhao J et al. proposed another strategy for lung division and knob identification by joining the highlights from CT and PET pictures. They utilized a unique edge-based division strategy to identify dubious zones. (Zhao et al., 2015). A help vector machine was utilized to order the knobs in the CT pictures through literary highlights. PET pictures were used to approve the technique.

In addition to knob highlights, Dr. Silvestri and his research group suggested proteomic classifiers to distinguish small-size considerate and hazardous lung knobs (Silvestri et al., 2018). They obtained impressive results on 8–30 mm knob sizes with a 40% decrease in biopsies on accommodating toggle switches.

In (Dou et al., 2017), the authors suggested 3D-CNN characterizing the volumetric generous and risky lung knobs to minimize the fake optimistic findings in a robotic lung knob recognition system in CT tests.

Subsequently, the ubiquity of convolutional neural systems (CNNs) in picture investigation, various sorts of network designs were proposed by analysts to expand the presentation of profound CNNs. As of recently, in the profound CNNs, thick geography structures ResNet, DenseNet (Huang et al., 2017), and DPNs execution is better as looked at than different ones. Yet, there is still space for association upgrades in these geographies (Chen et al., 2017). The MixNet design has developed association configurations with improved highlights of mining and diminished boundary excess (Wang et al., 2018).

3. Background:

Commonplace CAD frameworks for lung disease after writing partake the accompanying duct: picture preprocessing → discovery of carcinogenic knob applicants → knob up-and-comer false-positive decrease → threat expectation for every knob Competitor → danger forecast for by and large CT examine. These pipelines have numerous stages, every one of which is computationally costly and requires very much marked information during preparing. For instance, the bogus decisive decrease stage involves a set of data named valid & incorrect knob competitors, and the knob harm forecast stage requires a dataset with knobs marked with a threat.

Valid/False marks for knob up-and-comers and threat names for knobs are inadequate for lung Cancer growth. They might be nonexistent for some different tumors, so CAD frameworks that depend on such information would not sum up to various diseases. To achieve exceptional computational efficiency and generalizability for distinctive tumors, our CAD architecture would have a shorter pipeline and need the following details at some point in getting ready: a dataset of CT evaluations with accurate knobs labeled, and a dataset of CT philters with popular danger request. Best in class CAD frameworks that foresee harm from CT examines accomplish AUC of as much as 0.83. In any case, as referenced over, these frameworks take as information different named information that we don't utilize. We focus on our structure to arrive at near this exhibition.

4. Inspirations:

A lot of CT discusses investigative techniques that occur for lung knob discovery and order, which have an affectability of up to 94 percent, but with low peculiarity and high FP in knob structure. Then again, lung cancer development screening indicates that blood scans have greater explicitness and poorer affectability as opposed to MRI studies (Zamay et al., 2017). Unfortunately, there is no specific biomarker 100% touchy and clear for evaluating lung malignancy. There are a few types of biomarkers that are separated from inherited (transformations, variations in DNA and RNA articulation), proteomic (variations in plasma protein levels and coupling), and tumor proximity, efficiency improvement, and endothelial cells in the blood.

Dr. Silvestri and his exploration group have proposed proteomic classifiers to separate between little size kind and threatening knobs. They have planned a blood test by performing mass spectroscopy of the plasma proteins. Two proteins, named LG3BP and C163A, were distinguished as biomarkers for carcinogenic lung knob recognizable proof. The degree of these proteins in plasma, alongside five hazard factors, were utilized as classifiers and got impressive outcomes.

In contrast, the mix of numerous biomarkers gives high identification and finding ability. Albeit various PC based CT examine investigation strategies have preferable recognition execution over the radiologists, this despite everything doesn't address knobs of sizes <3 mm. Accordingly, an ultimate

conclusion concerning beginning phase lung Cancer growth analysis ought to be performed by utilizing numerous procedures, because roughly 60–80% of lung tumors are analyzed at advance stages.

Factor	Sensitivity (%age)	Specificity (%age)	NPV (%age)
Proteins LG3BP/C163A	97	13	95
Smoking history	97	<5	-
Age	97	8	92
Nodule size	100	13	100
Nodule location	97	<5	-
Nodule speculation	97	<5	-
Physiological symptoms	97	<5	-

Table 1. The relative contribution of risk factors with clinical biomarkers

5. State-of-the-art:

In this area, we portray a portion of the current lung disease, analytic ways to deal with order issues. In (Doi 2007), CADE and CADx frameworks dependent on the Hounsfield unit and play out the division by consolidating locale developing calculation and morphological channels. A ground-breaking learning model proposed in (Jadhav et al., 2015), which utilized a back-spread neural system for an order that would characterize the advanced X-beam, CT-pictures, MRIs, and so forth as malignant or non-dangerous. Further, a hereditary calculation has been utilized that concentrates include based on wellness work. The work introduced in (Krishnaiah et al., 2013), quickly looks at the expected utilization of grouping based information mining methods, for example, Rule-based, Decision tree, Naive Bayes, and Artificial Neural Network to a huge volume of social insurance information. The precision of the forecast looking at the two techniques is introduced. A multi-stage structure proposed in (Kumar et al., 2015) recognizes knobs in 3D lung CAT examines, decides whether every knob is harmful, and allots a disease likelihood dependent on these outcomes., a Histogram Equalization is utilized for pre-handling of the pictures and highlight extraction process and neural system classifier to check the state of a patient in its beginning phase whether it is typical or strange.

The work by Song (Song et al., 2017) presents a malignant growth grouping strategy by examining three sorts of profound neural systems (e.g., CNN, DNN, and SAE) which have been structured especially for lung disease arrangement. Those networks are

They are applied to the CT picture order task with specific changes for the benevolent and dangerous lung knobs. Another work for disease characterization in (Teramoto et al., 2017), which built up a computerized arrangement conspire for malignant lung growth introduced in infinitesimal pictures utilizing a profound convolutional neural net-work (dCNN), which is a significant, in-depth learning procedure.

The dCNN utilized for characterization comprises of three convolutional layers, three pooling layers, and two completely associated layers. The measurable boundaries like mean, standard deviation, skewness, kurtosis, fifth focal second, and 6th focal second are utilized for the order[11].

Taher (Taher & Sammouda, 2011) suggests two-division methods, Hopfield Neural Network (HNN) and Fuzzy C-Mean (FCM) bunching approximation for sputum shading photos to detect lung tumor in its early stages. Sputum test manual analysis is repetitive, off-base, and involves risky, trained individuals to retain a strategic detachment from suggestive blunders. A laptop-supported end (CAD)

system proposed in (Kuan et al., n. D.) utilizing deep highlights stripped from a vehicle encoder to organization lung knobs as both threatening and form. This study got the third place of the Kaggle lung malignant development. As far as we may know, it's also the key paper that presents the findings with proper analysis of those contested in Kaggle's rival. We introduce our research evaluation by adopting their testing protocol.

6. Suggested Network:

In this section, we present dCNN engineering in subtleties. Originally, we represent dCNN's general form and then explain our tragedy practice used to construct the conceptual dCNN model.

6.1. The Overall system:

The system starts with two convolution layers, in which the main convolution layer takes the picture with an input size of 120×120 pixels. The bit size for max-pooling segments is 2×2 and the step of 2 pixels and the completely associated layer creates a yield of 10 measurements. These ten yields are then passed to another layer containing 2 softmax units, which speak to the likelihood that the picture is providing of the lung malignancy or not. Every convolution layer in our dCNN model is trailed by a redressed direct unit (ReLU) layer to deliver their yields.

6.2. Loss Function:

We utilize *cross-entropy* as the misfortune capacity of our preparation model, which is figured by using a multinomial calculated relapse objective. This intends to boost the likelihood of patients with malignant growth by expanding the multinomial strategic relapse objective. In this paper, we accomplish this by limiting the cross-entropy misfortune for each preparation test. The preparation means to expand the likelihood of the real individual character by amplifying the multinomial strategic relapse objective. Hence, this is known as softmax misfortune work in our model. For a solitary info test x and a single yield hub I in the last layer, the misfortune could be determined by

$$p(y = i|x) = \frac{e^{a_i(x)}}{\sum_{i=1}^K e^{a_i(x)}} \tag{1}$$

Where $p(x)$ is approximated most extreme capacity, $a(x)$ is the actuation capacity of $x \in M$ with $M \subset Z^2$, and K is the number of classes (which is equivalent 2at this work). Lastly, the angles are figured by standard back-spread of the mistake (Hecht-Nielsen, 1988).

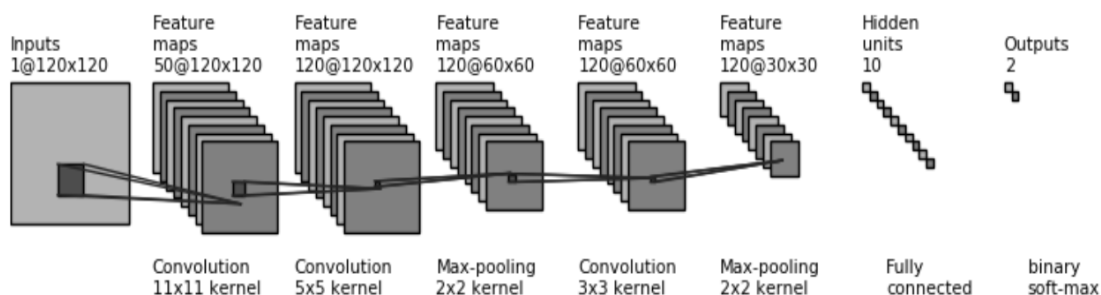


Fig 2: Shows Scheme of proposed dCNN architecture.

6.3. Performance estimations:

In clinical image analysis, a procedure shown is typically determined by peculiarity, affectability, and F1 performance.

Affectability quantifies the magnitude of true positive evaluations essentially identifying the degree of the hazardous knob correctly called contagious. Like this, the following description processes:

$$\text{sensitivity} = \frac{TP}{TP + FN} \quad (2)$$

Where TP (*True positive*) is the number of knobs that have been effectively-recognized, and FN (*false negative*) is the number of knobs that have been identified by the strategy. Interestingly, explicitness quantifies the extent of recognized negatives tests, in which the rate without dangerous knob is effectively delegated no carcinogenic. As such, particularity is processed as:

$$\text{specificity} = \frac{TN}{TN + FP} \quad (3)$$

Here TN (true negative) is the magnitude of noncancerous growth cases correctly described, and FP (false positive) is the magnitude of non-malignant growth patients incorrectly assigned.

Furthermore, F1-score quantifies the average F1 score through various class marks which are figured as:

$$F1 = 2 \times \frac{PPV \times TPR}{PPV + TPR} \quad (4)$$

Where PPV is

$$PPV = \frac{TP}{TP + FP} \quad (5)$$

And TPR is

$$TPR = \frac{TP}{TP + FN} \quad (6)$$

As introduced at the Kaggle rivalry, all outcomes by contenders ought to be given as the presentation estimation of log-misfortune work as follow:

$$\text{loss}(p, q) = -\frac{1}{|M|} \sum_{c \in M} w(c) \cdot p(c) \log q(c) \quad (7)$$

Where p is the genuine appropriation, F_c is the recurrence of class c in the smaller than usual group, and

$$w(c) = \begin{cases} \frac{f_{cancer-free}}{f_{cancer}} & \text{if } c \text{ belongs to the cancer class} \\ 1 & \text{Otherwise} \end{cases}$$

7. Experimental assessment:

We tested the dCNN model on the 2017 Kaggle Data Science Bowl (KDSB17) knowledge table, which was late provided for opposition to lung disease images. By presenting their findings, we have compared our outcome and different candidate.

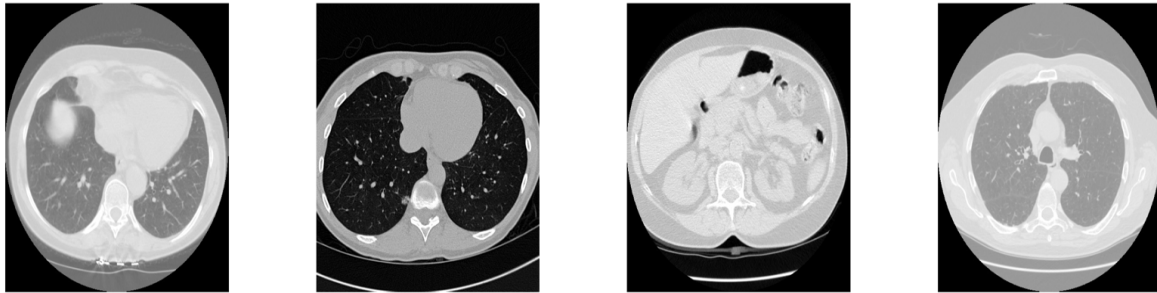


Fig 3: Four slices of different patient chests cavity from the Kaggle Data Science Bowl 2017 data set.

7. Information and Data:

The critical database is the person lung CT philter dataset from Kaggle's Data Science Bowl 2017. The dataset includes named details for 2101 individuals, which we divide into preparing size 1261, size 420 acceptance, and size 420 test collection. The details for each patient are CT review details and a label (0 for no cancer development, 1 for disease). Notice that the Kaggle dataset hasn't labeled knobs. For each case, the CT analyses details comprising a variable number of pictures (usually about 100-400, each image is a hub cut) of 512/512 pixels. Cuts are in the DICOM community. About 70% of the names provided in the Kaggle dataset are 0, so we use a calculated failure function in our threat classifier to fix this discomfort.

Since the Kaggle dataset alone ends up failing to reliably classify the acceptance range, we also use the Lung Nodule Analysis 2016 patient lung CT philter dataset called knobs to prepare a U-Net for lung knob identification. The LUNA16 dataset includes identified details for 888 individuals, separated into a size 710 planning set and size 178 acceptance set. For each case, CT details explore knowledge and a knob label (rundown of knob oriented directions and breadth). The CT philter details for each patient is a variable number of pictures (regularly about 100-400, each image is a hub cut) of 512/512 pixels.

LUNA16 knowledge was used to create a knob recognition U-Net, one of the steps in our pipeline. The problem is to specifically determine the name of a patient ('Cancer development' or 'no disease') provided the patient's Kaggle lung CT test. We will use ROC's accuracy, affectability, peculiarity, and AUC to determine the appearance of our CAD system on the Kaggle test collection.

8. Methods:

We define the following 3D CT explores separation, standardization, downsampling, and extremely low-focusing. Our fundamental approach was to notify 3D CT preprocessed tests into 3D CNNs. Yet the results were bad, so we wanted to preprocess to reach only points of focus in 3D CNNs. To identify areas of mystery, we practice a knob opponent recognition U-net. At that point, we insert districts around knob competitors listed in 3D CNNs by the U-net to finally organize CT checks as positive or negative for lung cancer development. Our system layout and weight-saving techniques are focused on CS224N Winter 2016 Allocation 4 Starter Technology.

8.1. Pre-processing and Segmentation:

With each case, we first proselytize pixel articulations in each picture to Hounsfield units (HU), a radio thickness calculation, and frame 2D cuts in a single 3D picture. Since tumors build on lung tissue, we use division to cover the bone, outside air, and multiple substances that render our details noisy and leave only lung tissue details for the classifier. Several classification methods were taken, including thresholding, grouping (K-means and Meanshift), and Watershed. Next to no control, K-means and Mean-move for no outstanding subjective performance. Catchment produced the strongest personal skill, but it took too long to conceive about racing for cutoff time. Ultimately, our pipeline used the threshold method. Quantization and Drainage are listed below.

After separation, we standardize the 3D image by using vertical scaling to force all pixels of the first unsegmented image to values between 0 and 1. At that point, we use spline interjection to downsample every 3D image by size of 0.5 in every one of the three measurements. At long last, we zero-focus the information be taking away the mean of the considerable number of pictures from the preparation set.

8.1.1. Thresholding:

Popular broadcast-densities of different CT philter parts appear in Table 2. Air is normally about -1000 HU, lung tissue is typically about -500 , skin, blood and other tissues are around 0 HU, and bone is generally about 700 HU, but we cover pixels around -1000 or above -320 to leave lung tissue as the core component. Pixel dispersion Hounsfield units at various critical cuts; constant, for example, occurs in Figure 4. Figure 5 indicates the 400 HU pixel level. Figure 6 executes the mask. However, to reflect the possibility that any disruptive development may occur inside the bronchioles (airways) within the lung performed in Figure 7, we decide to add this air to create the finished veil as seen in Figure 8.

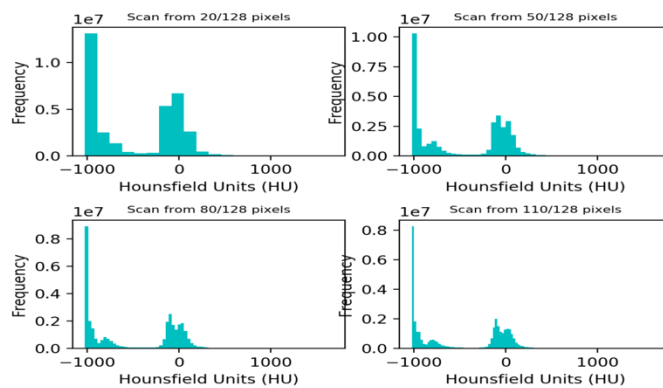
Substance	Radiodensity (HU)
Air	-1000
Lung tissue	-500
water and blood	0
bone	700

Table 2: Shows typical radio densities in HU of various substances in a CT scan

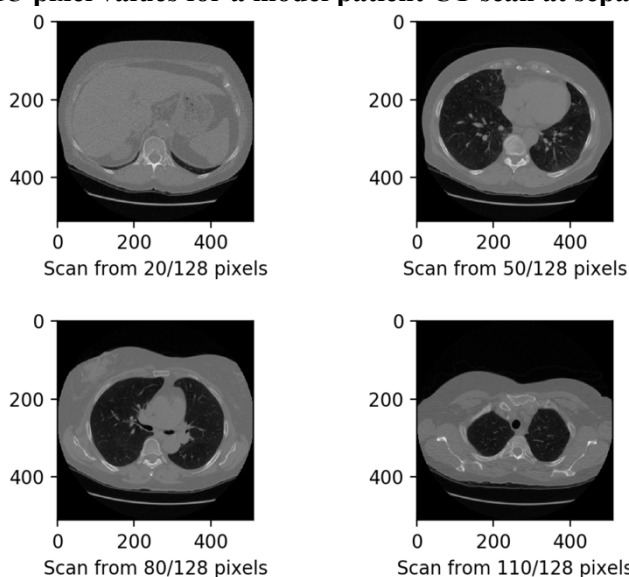
8.1.2. Watershed:

The unit gained from segmentation is rather agitated. Various samples that were a piece of lung tissue, particularly pixel values at the center of the lung, will usually fall beyond the lung tissue radio-thickness due to CT philter clamor. This ensures that our definition statesn't have the choice to easily group pictures where unsafe knobs are at the edges of the lung. Designers use market-driven watershed division to channel commotion and insert pixel values from the sides, as seen in Al-Tarawneh. A special 2D CT resistant cut is seen in Figure 9. The resulting 2D cut of the lung division veil rendered by thresholding occurs in Figure 10, and the corresponding 2D decrease in Watershed's lung division cover is shown in Figure 11. Subjectively, this allows slightly greater separation than thresholding. Missing voxels (dark specks in Figure 10) are mostly re-included. However, this is

substantially less competent than critical thresholds, but due to time constraints, we could not pre-process all CT tests using Watershed, so we used thresholds.



a) images of HU pixel values for a model patient CT scan at separate sections.



b) Corresponding 2D axial slices

Figure 4: (a) Histogram of HU values at (b) corresponding axial slices for study patient 3D picture at separate axial slices

8.2. U-Net for Nodule Detection:

At first, we tried to add all the broken lungs to the threat classifiers. The findings, however, were weak. The whole image might have been too big a pursuit room. We need, along these lines, a method of contributing excitement to littler districts rather than the entire portioned 3D picture. Our method is picking tiny boxes containing potential carcinogenic knob competitors. To find these top up-and-comers knobs, we train an altered U-Net variant on LUNA16 data in Ronneberger (Ronneberger et al., 2015). U-Net is a 2D CNN tech for the biomedical image group. We designed U-Net 's stripped-down implementation to restrict memory usage. For Figure 13, a description of our U-Net engineering is remembered and described in Table 3. In planning, our modified U-Net takes as details 256 / 256 2D CT cuts, and names are provided (256256 veils where knob pixels are 1, rest 0).

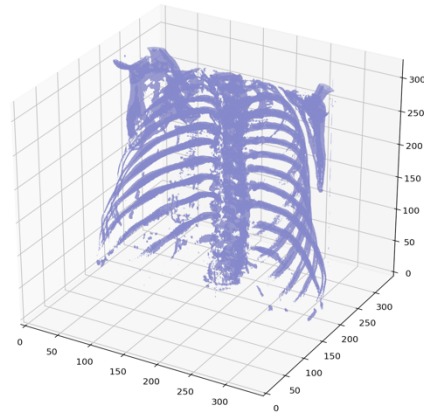


Fig 5: A reference 3D image of a patient with values greater than 400HU shows a bone fragment.

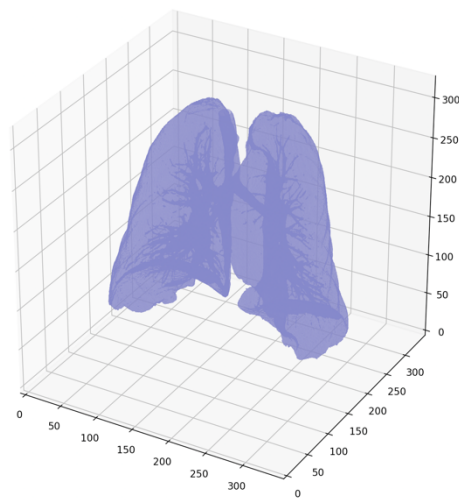


Fig 6: Sample patient initial mask with no air

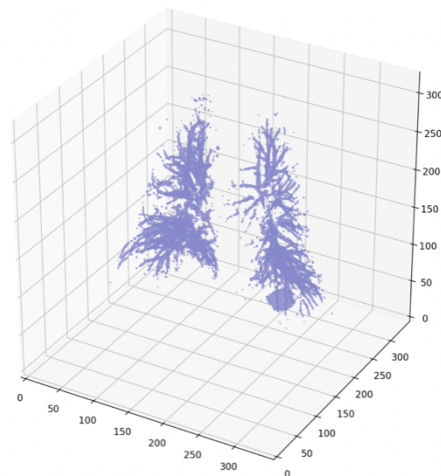


Fig 7: Sample patient bronchioles within the lung

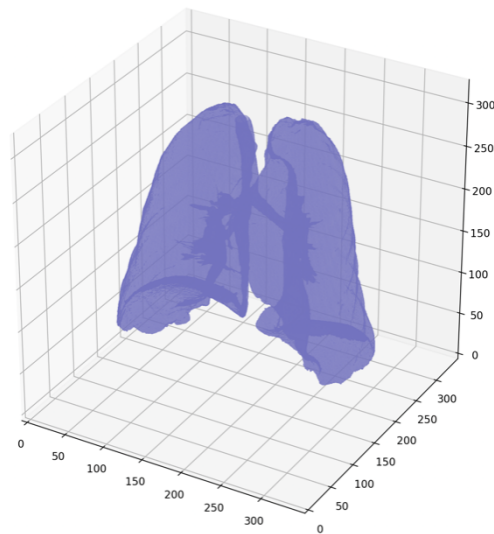


Fig 8: Sample patient final mask in which bronchioles are included

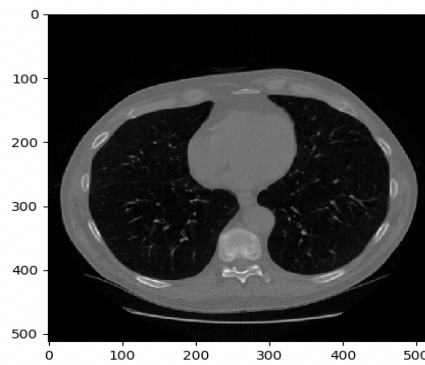


Fig 9: an original 2D slice of sample patient

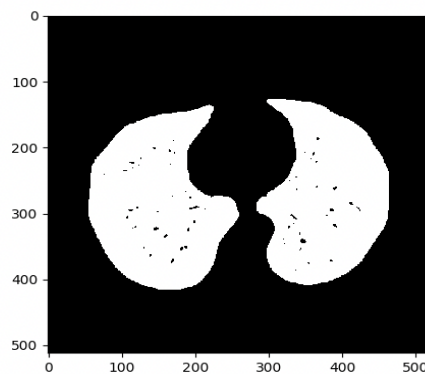


Fig 10: lung segmentation mask by thresholding of sample patient

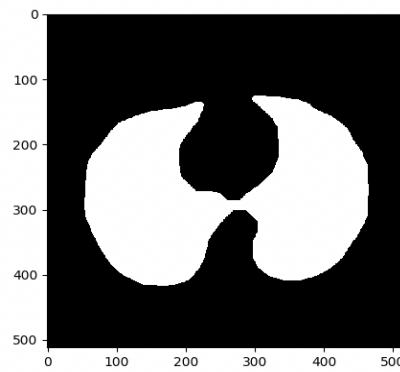


Fig 11: final watershed segmentation mask of sample patient

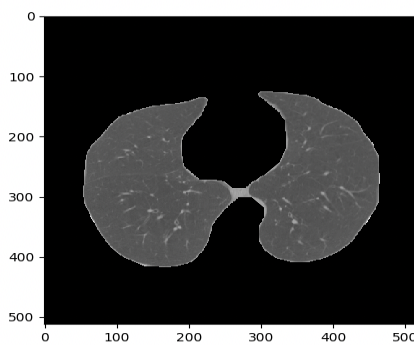


Fig 12: final watershed lung segmentation of sample patient

The model is prepared to yield pictures of shape 256×256 Where any pixel of yield has an opportunity anywhere in the range between 0 and 1, indicating the probability that the pixel would have a position with a knob. This is achieved by taking the cut relating to the name of one of the softmax of the last U-Net row. Trying to relate U-Net inputs, marks, and goals for the LUNA16 patient are seen separately in Figures 14, 15, and 16. Most knobs are far smaller than the weighted softmax cross-entropy folly calculated for each node since the label of 0 is unmistakably more prominent in the cover than the symbol of 1. To generate knob candidates, the prepared U-Net is then added to the portioned Kaggle CT filtering cuts.

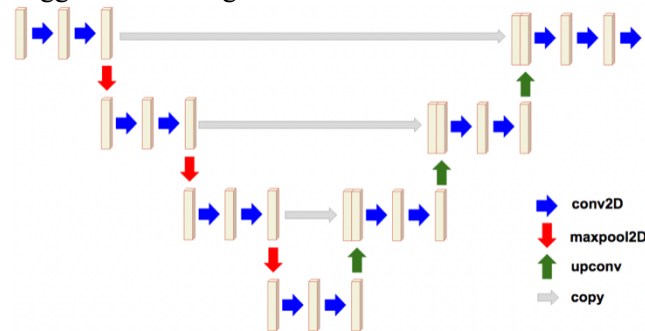


Fig 13: Modified U-Net architecture

Layer	Params	Activation	Output
Input			256 x 256 x 1
Conv1a	3x3x3	ReLu	256 x 256 x 32
Conv1b	3x3x3	ReLu	256 x 256 x 32
Max Pool	2x2, stride 2		128 x 128 x 32
Conv2a	3x3x3	ReLu	128 x 128 x 80
Conv2b	3x3x3	ReLu	128 x 128 x 80
Max Pool	2x2, stride 2		64 x 64 x 80
Conv3a	3x3x3	ReLu	64 x 64 x 160
Conv3b	3x3x3	ReLu	64 x 64 x 160
Max Pool	2x2, stride 2		32 x 32 x 160
Conv4a	3x3x3	ReLu	32 x 32 x 320
Conv4b	3x3x3	ReLu	32 x 32 x 320
Up Conv4b	2x2		64 x 64 x 320
Concat	Conv4b,Conv3b		64 x 64 x 480
Conv5a	3x3x3	ReLu	64 x 64 x 160
Conv5b	3x3x3	ReLu	64 x 64 x 160
Up Conv5b	2x2		128 x 128 x 160
Concat	Conv5b,Conv2b		128 x 128 x 240
Conv6a	3x3x3	ReLu	128 x 128 x 80
Conv6b	3x3x3	ReLu	128 x 128 x 80
Up Conv6b	2x2		256 x 256 x 80
Concat	Conv6b,Conv1b		256 x 256 x 112
Conv6a	3x3x3	ReLu	256 x 256 x 32
Conv6b	3x3x3	ReLu	256 x 256 x 32
Conv7	3x3x3		256 x 256 x 2

Table 3: U-Net design (Dropout with 0.2 likelihood after each 'a' conv sheet, 'Up' indicates image resizing through bilinear interpolation, Adam Optimizer, learning rate = 0.0001)

8.3. Cancer Classifiers:

As we planned the U-Net on LUNA16 details, we run it on Kaggle details 2D cuts and stacked the 2D cuts back to build up-and-comers knob. In an ideal future, U-Net yield will give us the particular areas of a significant amount of knobs, and we would have the choice to say pictures with knobs as defined by U-Net are positive for lung malignancy, and pictures without U-Net classified knobs are negative for lung disease. Notwithstanding, as seen in Figure 14, U-Net offers a positive sign for the actual knob, but additionally produces several fake positives, so we need an extra classifier to determine the damage. As our U-Net generates more questionable areas than real knobs, we find the strongest eight applicants ($32 \times 32 \times 32$ volumes) Sliding the knowledge window and spared the eight typically actuated (most popular L2) parts. To prevent essentially combining the highest divisions in the picture's most glorious city, the eight areas we ultimately selected were not authorized to overlap each other. We then combined these regions into one $64 \times 64 \times 64$ pictures, which will fill in as the contribution to our classifiers, which relegate a name to the image (Cancer growth or not disease). [37-41]

We use a simple labeling scale, a standard 3D CNN, and a Googlenet-based 3D CNN. Each of our classifiers uses weighted softmax cross-entropy misfortune (weight for a label is the opposite of the name recurrence in the preparation set) and Adam Optimizer, and CNN's use ReLU enactment and dropout after each convolutional layers throughout the planning. Vanilla 3D CNN relies on de-finished 3D CNN documentation for this task. We hired the device to overburden the relatively limited Kaggle dataset. For Figure 17, our vanilla 3D CNN style experience is remembered and described in Table 5.

We have designed a Googlenet-assembled 3D model focused on the 2D model intended for picture order in Szegedy et al. (Szegedy et al., 2015). For Figure 18, a description of our Googlenet 3D is remembered and described in Table 6. Refer Szegedy for more launch module details (Szegedy et al., 2015).

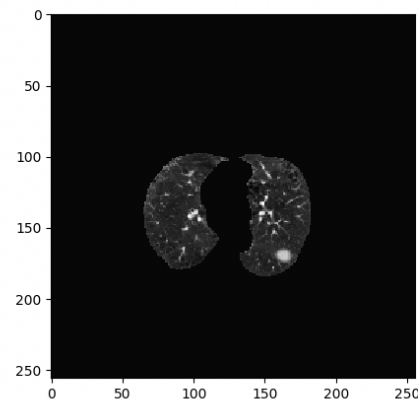


Figure 14: U-Net validation collection sample data of LUNA16.

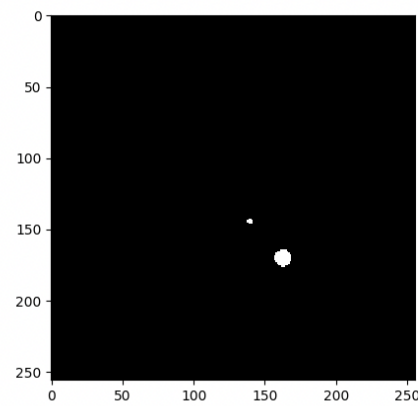


Figure 15: U-Net specimen labeling LUNA16 testing collection with the position of the underlying data nodule

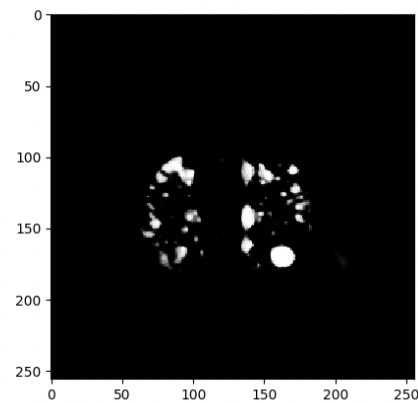


Figure 16: U-Net projected LUNA16 validated performance.

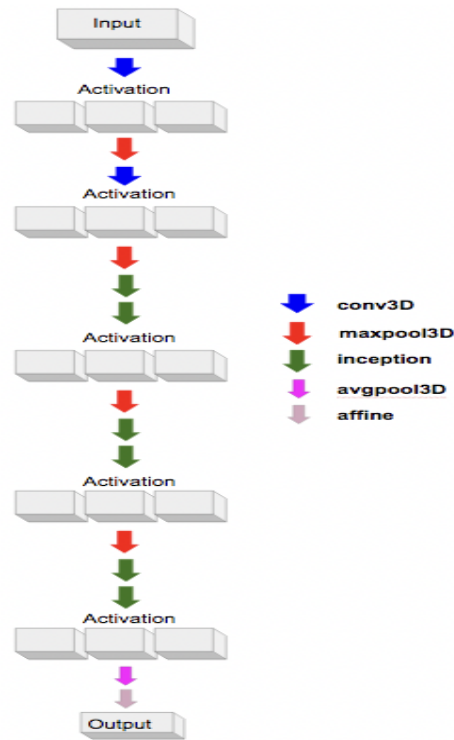


Fig 18: 3D google net architecture

Layer	Params	Activation	Output
Input			64 x 64 x 64 x 1
Conv1	7x7x7	ReLu	32 x 32 x 32 x 32
MaxPool	2x2x2		16 x 16 x 16 x 32
Conv2	3x3x3	ReLu	16 x 16 x 16 x 64
MaxPool	2x2x2		8 x 8 x 8 x 64
Inception1	1,3,5	ReLu	8 x 8 x 8 x 128
Inception2	1,3,5	ReLu	8 x 8 x 8 x 128
MaxPool	2x2x2		4 x 4 x 4 x 128
Inception3	1,3,5	ReLu	4 x 4 x 4 x 256
Inception4	1,3,5	ReLu	4 x 4 x 4 x 256
MaxPool	2x2x2		2 x 2 x 2 x 256
Inception5	1,3,5	ReLu	2 x 2 x 2 x 512
Inception6	1,3,5	ReLu	2 x 2 x 2 x 512
AvgPool	2x2x2	ReLu	1 x 1 x 1 x 512
Dense			2

Table 6: 3D Google Design (dropout 0.3 likelihood for each Conv and start layer during preparation, Adam Optimizer with learning rate = 0.0001)

Model	Acc.	Sens.	Spec.	AUC
Linear	0.665	0.652	0.672	0.663
Vanilla 3D CNN	0.705	0.593	0.761	0.695
3D Googlenet	0.751	0.770	0.741	0.757

Table 7: Kaggle test set accuracy, sensitivity, specificity, and AUC of ROC (not shown for linear)

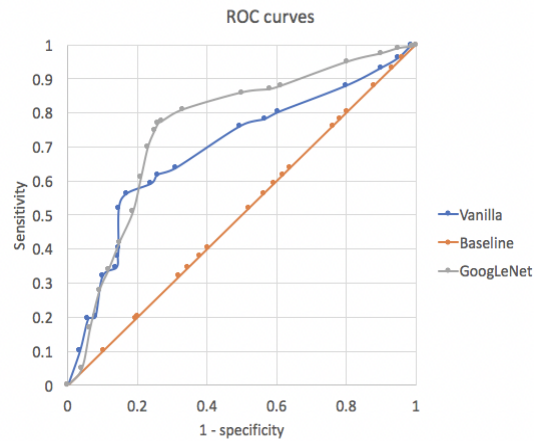


Fig 19: ROC for Vanilla 3D CNN and 3D Googlenet

10. Conclusion:

The profound 3D CNN models, accurately the Googlenet-based model, played out the best on the test set. While we Will does not do the best in class AUC 0.83 implementation, we're well worried about utilizing fewer called details than the best in class CAD systems. As a curious experience, the first actuation layer of one of our more developed models (where we insert the entire CT volume) for an ex-abundant acceptance called positive for disease is displayed in figure 20. The splendid pixels as a rule related to the area of harmful knobs, so it could be conceivable to extend our present model not just to decide if the patient has cancer growth, yet besides, choose the specific area of the dangerous knobs. The most short term work is to utilize Watershed division as the underlying lung division. Different open doors for development incorporate the creation of the system more profound, and broader hyper-boundary tuning.

Additionally, we spared our model boundaries, best case scenario approval AUC, yet maybe we could have saved at different measurements, for example, F1. Other future works incorporate stretching out our models to 3D pictures for different diseases. The upside of not requiring an excessive amount of marked information explicit to our malignancy is it could make it generalizable to various tumors.

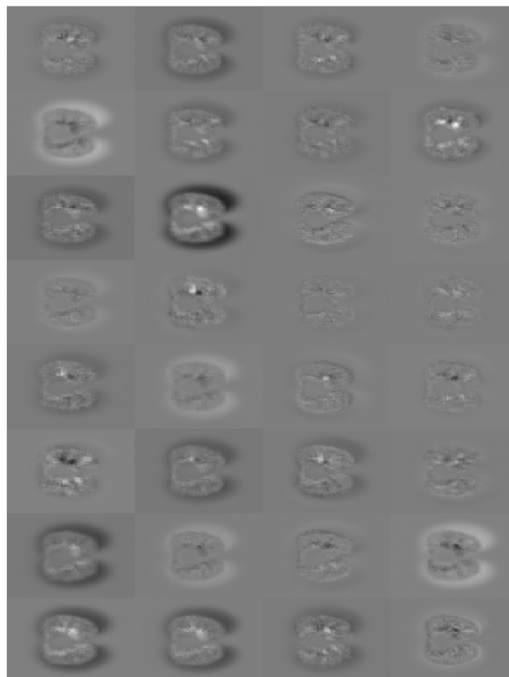


Figure 20: events revealing cancerous nodule in certain outlets

11. References:

1. *Lung Cancer Detection Using Image Processing Techniques*. (n.d.). Retrieved August 13, 2020, from https://www.researchgate.net/publication/265998089_Lung_Cancer_Detection_Using_Image_Processing_Techniques
2. *2nd place solution for the 2017 national data science bowl – Julian de Wit – Freelance software/machine learning engineer*. (n.d.). Retrieved August 13, 2020, from <http://juliandewit.github.io/kaggle-nds2017/>
3. Chen, Y., Li, J., Xiao, H., Jin, X., Yan, S., & Feng, J. (2017). *Dual-Path Networks*.
4. *Data - LUNA16 - Grand Challenge*. (n.d.). Retrieved August 13, 2020, from <https://luna16.grand-challenge.org/Data/>
5. *Data Science Bowl 2017 - The Cancer Imaging Archive (TCIA) Public Access - Cancer Imaging Archive Wiki*. (n.d.). Retrieved August 13, 2020, from <https://wiki.cancerimagingarchive.net/display/Public/Data+Science+Bowl+2017>
6. Doi, K. (2007). Computer-aided diagnosis in medical imaging: historical review, current status, and future potential. *Computerized Medical Imaging and Graphics*, 31(4–5), 198–211. <https://doi.org/10.1016/j.compmedimag.2007.02.002>
7. Dou, Q., Chen, H., Yu, L., Qin, J., & Heng, P. A. (2017). Multilevel Contextual 3-D CNNs for False Positive Reduction in Pulmonary Nodule Detection. *IEEE Transactions on Biomedical Engineering*, 64(7), 1558–1567. <https://doi.org/10.1109/TBME.2016.2613502>
8. *Early detection of lung cancer | F1000Research*. (n.d.). Retrieved August 13, 2020, from <https://f1000research.com/articles/5-739>
9. Ferlay, J., Soerjomataram, I., Dikshit, R., Eser, S., Mathers, C., Rebelo, M., Parkin, D. M., Forman, D., & Bray, F. (2015). Cancer incidence and mortality worldwide: Sources, methods, and major patterns in GLOBOCAN 2012. *International Journal of Cancer*, 136(5), E359–E386. <https://doi.org/10.1002/ijc.29210>
10. GHO | By category. (n.d.-a). *WHO*.
11. *GHO | By category*. (n.d.-b). Retrieved August 13, 2020, from <https://apps.who.int/gho/data/view.main>
12. Hecht-Nielsen, R. (1988). Theory of the backpropagation neural network. *Neural Networks*, 1(1 SUPPL), 445. [https://doi.org/10.1016/0893-6080\(88\)90469-8](https://doi.org/10.1016/0893-6080(88)90469-8)
13. Huang, G., Liu, Z., Van Der Maaten, L., & Weinberger, K. Q. (2017). Densely connected convolutional networks. *Proceedings - 30th IEEE Conference on Computer Vision and Pattern Recognition, CVPR 2017, 2017-January*, 2261–2269. <https://doi.org/10.1109/CVPR.2017.243>
14. Jadhav, A., Dighe, A., Chavan, V., & Patil, D. Y. (2015). *Detection of Lung Cancer Using Backpropagation Neural Networks and Genetic Algorithm*. www.ijcta.com
15. Jemal Lindsey Torre Isabelle Soerjomataram Freddie Bray, A., & Adams, C. (n.d.). *Third Edition THE CANCER ATLAS Third Edition THE CANCER ATLAS 4 5*. Retrieved August 13, 2020, from www.cancer.org
16. Jiang, H., Ma, H., Qian, W., Gao, M., & Li, Y. (2018). An Automatic Detection System of Lung Nodule Based on Multigroup Patch-Based Deep Learning Network. *IEEE Journal of Biomedical and Health Informatics*, 22(4), 1227–1237. <https://doi.org/10.1109/JBHI.2017.2725903>
17. Krishnaiah, V., Narsimha, G., & Chandra, N. S. (2013). *Diagnosis of Lung Cancer Prediction System Using Data Mining Classification Techniques*.
18. Kuan, K., Ravaut, M., Manek, G., Chiang Howe, T., Radiology, C., Zeng, Z., & Chandrasekhar, V. (n.d.). *Deep Learning for Lung Cancer Detection: Tackling the Kaggle Data Science Bowl 2017 Challenge*.
19. Kumar, D., Wong, A., & Clausi, D. A. (2015). Lung Nodule Classification Using Deep Features in CT Images. *Proceedings -2015 12th Conference on Computer and Robot Vision, CRV 2015*, 133–138. <https://doi.org/10.1109/CRV.2015.25>
20. *LUNG CANCER DETECTION AND PREDICTION BY USING NEURAL NETWORK, Authors: Raviprakash S. Shriwas, Akshay D. Dikondawar, IPASJ INTERNATIONAL*

- JOURNAL OF ELECTRONICS & COMMUNICATION (IJEC)*, <http://www.ipasj.org/IJEC/IJEC.htm>. (n.d.). Retrieved August 13, 2020, from https://www.ipasj.org/pabstract_Share.php?pid=IJEC-2015-01-11-6
21. Midthun, D. E. (2016). Early detection of lung cancer. In *F1000Research* (Vol. 5, p. 739). Faculty of 1000 Ltd. <https://doi.org/10.12688/f1000research.7313.1>
 22. Ren, S., He, K., Girshick, R., & Sun, J. (2017). Faster R-CNN: Towards Real-Time Object Detection with Region Proposal Networks. *IEEE Transactions on Pattern Analysis and Machine Intelligence*, 39(6), 1137–1149. <https://doi.org/10.1109/TPAMI.2016.2577031>
 23. Ronneberger, O., Fischer, P., & Brox, T. (2015). U-net: Convolutional networks for biomedical image segmentation. *Lecture Notes in Computer Science (Including Subseries Lecture Notes in Artificial Intelligence and Lecture Notes in Bioinformatics)*, 9351, 234–241. https://doi.org/10.1007/978-3-319-24574-4_28
 24. Setio, A. A. A., Traverso, A., de Bel, T., Berens, M. S. N., Bogaard, C. van den, Cerello, P., Chen, H., Dou, Q., Fantacci, M. E., Geurts, B., Gugten, R. van der, Heng, P. A., Jansen, B., de Kaste, M. M. J., Kotov, V., Lin, J. Y. H., Manders, J. T. M. C., Sónora-Mengana, A., García-Naranjo, J. C., ... Jacobs, C. (2017). Validation, comparison, and combination of algorithms for automatic detection of pulmonary nodules in computed tomography images: The LUNA16 challenge. *Medical Image Analysis*, 42, 1–13. <https://doi.org/10.1016/j.media.2017.06.015>
 25. Siegel, R., DeSantis, C., & Jemal, A. (2014). Colorectal cancer statistics, 2014. *CA: A Cancer Journal for Clinicians*, 64(2), 104–117. <https://doi.org/10.3322/caac.21220>
 26. Silvestri, G. A., Tanner, N. T., Kearney, P., Vachani, A., Massion, P. P., Porter, A., Springmeyer, S. C., Fang, K. C., Midthun, D., & Mazzone, P. J. (2018). Assessment of Plasma Proteomics Biomarker's Ability to Distinguish Benign From Malignant Lung Nodules: Results of the PANOPTIC (Pulmonary Nodule Plasma Proteomic Classifier) Trial. *Chest*, 154(3), 491–500. <https://doi.org/10.1016/j.chest.2018.02.012>
 27. Song, Q. Z., Zhao, L., Luo, X. K., & Dou, X. C. (2017). Using Deep Learning for Classification of Lung Nodules on Computed Tomography Images. *Journal of Healthcare Engineering*, 2017. <https://doi.org/10.1155/2017/8314740>
 28. Szegedy, C., Liu, W., Jia, Y., Sermanet, P., Reed, S., Anguelov, D., Erhan, D., Vanhoucke, V., & Rabinovich, A. (2015). Going deeper with convolutions. *Proceedings of the IEEE Computer Society Conference on Computer Vision and Pattern Recognition, 07-12-June-2015*, 1–9. <https://doi.org/10.1109/CVPR.2015.7298594>
 29. Taher, F., & Sammouda, R. (2011). Lung cancer detection by using artificial neural network and fuzzy clustering methods. *2011 IEEE GCC Conference and Exhibition, GCC 2011*, 295–298. <https://doi.org/10.1109/IEEGCC.2011.5752535>
 30. Teramoto, A., Tsukamoto, T., Kiriya, Y., & Fujita, H. (2017). Automated Classification of Lung Cancer Types from Cytological Images Using Deep Convolutional Neural Networks. *BioMed Research International*, 2017. <https://doi.org/10.1155/2017/4067832>
 31. Veronesi, G., Maisonneuve, P., Spaggiari, L., Rampinelli, C., Pardolesi, A., Bertolotti, R., Filippi, N., & Bellomi, M. (2014). Diagnostic performance of low-dose computed tomography screening for lung cancer over five years. *Journal of Thoracic Oncology*, 9(7), 935–939. <https://doi.org/10.1097/JTO.0000000000000200>
 32. Wang, W., Li, X., Lu, T., & Yang, J. (2018). Mixed link networks. *IJCAI International Joint Conference on Artificial Intelligence, 2018-July*, 2819–2825. <https://doi.org/10.24963/ijcai.2018/391>
 33. Y., G., X., L., L., Y., B., Z., D., Y., Y., Z., L., G., L., W., T., Z., Gu, Y., Lu, X., Yang, L., Zhang, B., Yu, D., Zhao, Y., Gao, L., Wu, L., & Zhou, T. (2018). Automatic lung nodule detection using a 3D deep convolutional neural network combined with a multiscale prediction strategy in chest CTs. *Computers in Biology and Medicine*, 103, 220–231. <https://doi.org/10.1016/j.compbio.2018.10.011> LK
http://elinks.library.upenn.edu/sfx_local?sid=EMBASE&issn=18790534&id=doi:10.1016%2Fj.compbio.2018.10.011&atitle=Automatic+lung+nodule+detection+using+a+3D+dee+p+convolutional+neural+network+combined+with+a+multi-scale+prediction+strategy+in+chest+CTs&title=Comput.+Biol.+Med.&title=Computers+in

- +Biology+and+Medicine&volume=103&issue=&spage=220&epage=231&aualast=Gu&aufirst=Yu&aunit=Y.&aufull=Gu+Y.&coden=CBMDA&isbn=&pages=220-231&date=2018&aunit1=Y&aunitm
34. Zamay, T. N., Zamay, G. S., Kolovskaya, O. S., Zukov, R. A., Petrova, M. M., Gargaun, A., Berezovski, M. V., & Kichkailo, A. S. (2017). Current and prospective protein biomarkers of lung cancer. In *Cancers* (Vol. 9, Issue 11). MDPI AG. <https://doi.org/10.3390/cancers9110155>
 35. Zhao, J., Ji, G., Qiang, Y., Han, X., Pei, B., & Shi, Z. (2015). A New Method of Detecting Pulmonary Nodules with PET/CT Based on an Improved Watershed Algorithm. *PLOS ONE*, 10(4), e0123694. <https://doi.org/10.1371/journal.pone.0123694>
 36. Zhu, W., Liu, C., Fan, W., & Xie, X. (2018). DeepLung: Deep 3D dual-path nets for automated pulmonary nodule detection and classification. *Proceedings - 2018 IEEE Winter Conference on Applications of Computer Vision, WACV 2018, 2018-January*, 673–681. <https://doi.org/10.1109/WACV.2018.00079>
 37. Rohit Raja, Sandeep Kumar, Md Rashid, Color Object Detection Based Image Retrieval using ROI Segmentation with Multi-Feature Method, in *Wireless Personal Communication Springer Journal*, Print ISSN0929-6212 online ISSN1572-834 pp-1-24, <https://doi.org/10.1007/s11277-019-07021-6>.
 38. Ramakant Chandrakar, Rohit Raja, Rohit Miri, S R Tandan, K. Ramya Laxmi, Detection and Identification of Animals in Wild Life Sanctuaries using Convolutional Neural Network, 'International Journal of Recent Technology and Engineering (IJRTE)' that will publish at Volume-8 Issue-5, January 2020 in Regular Issue on January 30, 2020.
 39. Sumati Pathak, **Rohit Raja**, Vaibhav Sharma, Srinivas Ambala, ICT Utilization and Improving Student Performance in Higher Education, *International Journal of Recent Technology and Engineering (IJRTE)* at Volume-8 Issue-2, pp. 5120-5124, July 2019.
 40. Laxmikant Tiwari, **Rohit Raja**, Vaibhav Sharma, Rohit Miri, Adaptive Neuro-Fuzzy Inference System Based Fusion Of Medical Image, *International Journal Of Research In Electronics And Computer Engineering*, Vol 7, Iss. 2, pp. 2086-2091, ISSN: 2393-9028 (PRINT) |ISSN: 2348-2281 (ONLINE).
 41. Sumati Pathak, **Rohit Raja**, Vaibhav Sharma, and K. Ramya Laxmi, A Framework Of ICT Implementation On Higher Educational Institution With Data Mining Approach, *European Journal of Engineering Research and Science*, ISSN (Online): 2506-8016